A robust method for calculating interface curvature and normal vectors using an extracted local level set

Åsmund Ervik[a,b,*], Karl Yngve Lervåg[b], Svend Tollak Munkejord[a]

[a]*SINTEF Energy Research, P.O. Box 4761 Sluppen, NO-7465 Trondheim, Norway*
[b]*NTNU, Department of Energy and Process Engineering, Kolbjørn Hejes v 1B, NO-7491 Trondheim, Norway*

Abstract

The level-set method is a popular interface tracking method in two-phase flow simulations. An often-cited reason for using it is that the method naturally handles topological changes in the interface, e.g. merging drops, due to the implicit formulation. It is also said that the interface curvature and normal vectors are easily calculated. This last point is not, however, the case in the moments during a topological change, as several authors have already pointed out. Various methods have been employed to circumvent the problem. In this paper, we present a new such method which retains the implicit level-set representation of the surface and handles general interface configurations. It is demonstrated that the method extends easily to 3D. The method is validated on static interface configurations, and then applied to two-phase flow simulations where the method outperforms the standard method and the results agree well with experiments.

Keywords: Level-Set Method, Curvature, Normal vector, Droplet-film interaction

1. Introduction

Investigations of droplet collision phenomena have a long tradition in the study of multiphase flow, dating back to Lord Rayleigh [1] who in 1879 noted that a raindrop can bounce off a pool, and to Worthington [2] who in 1876 studied among other things the central jet that now bears his name. The early work predates the rise of computational studies, and consists of experimental studies that enabled a separation of the flow patterns into various regimes characterized by e.g. the Weber number and Ohnesorge number. A case which has long been the focus of study is that of a single droplet of one liquid, immersed in some other gas or liquid, and which collides with a deep pool of the first liquid. This could be e.g. a raindrop falling onto a pond, or a droplet of Liquefied Natural Gas (LNG) merging with a pool of LNG in a liquefaction heat exchanger, so the case is interesting also from an industry point of view. Such a system may seem simple at first, but experimental and numerical studies have shown that varied phenomena such

[*]Corresponding author
Email addresses: `asmund.ervik@sintef.no` (Åsmund Ervik), `karl.y.lervag@ntnu.no` (Karl Yngve Lervåg), `svend.t.munkejord@sintef.no` (Svend Tollak Munkejord)

as coalescence, bouncing, jetting and partial merging occur. The system is also not fully understood yet; as an example, Thoroddsen et al. [3] have recently shown that for high impact velocities a turbulent boundary layer forms between the droplet and the pool after they merge.

In order to study such a case using computer simulations, it is necessary to use a precise interface-tracking method to capture the physics before, during and after the collision. The Level-Set Method (LSM) is a popular choice for interface tracking in studies of collisions, since its implicit formulation means that the method can handle the topological change which occurs when two interfaces merge. The LSM is very general, and apart from fluid dynamics it has been used for modelling such diverse phenomena as tumor growth [4], wildland fire propagation [5] and computer RAM production [6]. For a good introduction to the LSM, see e.g. [7]. The LSM originated from the seminal article by Osher and Sethian [8].

In two-phase flow simulations using the LSM, accurate interface curvature and normal vector information is vital in order to get good results. Standard methods exist for calculating these geometric quantities, but they fail when the interface topology changes, e.g. when two drops collide and merge. Several approaches have been used to remedy this flaw. The first approach to this problem is described by Smereka in [9]. He describes the problem briefly, and increases the numerical smoothing in the curvature discretization to lessen the effect. This is not an optimal solution, and Smereka notes on one of the simulations with merging interfaces that "most of the area loss occurs at the topology change". Several non-smearing approaches have subsequently been developed, by Macklin and Lowengrub [4, 10], by Salac and Lu [11] and by Lervåg [12, 13]. The methods by Macklin and Lowengrub and by Lervåg use curve fitting to obtain an accurate representation of the interface, while the method by Salac and Lu extracts several level-set functions each representing only a single body, and uses these to calculate the curvature.

The present work proposes a new method, which is an extension of previous methods, for calculating the curvature and normal vectors. The proposed method is based on the method by Salac and Lu, but it handles more general interface configurations and topological changes, as it considers only the local area around a point. The quality function introduced by Macklin and Lowengrub is used to restrict the use of the proposed method to those areas where it is needed, thus reducing the computational cost. As the proposed method uses no curve fitting, it extends easily to three dimensions, as demonstrated here. The proposed method is compared to the standard method for demanding cases where the analytical curvature is known; for such a case the proposed method gives errors of 1–2% where the standard method gives errors of $\mathcal{O}(1/\Delta x) > 100\%$. The proposed method is based on the work of Ervik [14].

The outline of this work is as follows: In Section 2, the theory of two-phase incompressible flow, the LSM and numerical methods are briefly reviewed. In Section 3, the proposed method is presented in detail. In Section 4, the method is validated on geometric test cases, and the results are compared to other methods. In Section 5, the results of two-phase flow simulations using the current method are reported and compared to experimental results. Finally, in Section 6, some concluding remarks are offered.

2. The Level-Set Method and two-phase flow

The LSM is one of the more successful interface-capturing methods used in computational physics. Since its introduction by Osher and Sethian in [8], it has been used for numerous physical applications, as well as in computer graphics. Perhaps the main virtue of the LSM is how intuitive it is; in 2D it can easily be explained to anyone with a basic knowledge of multivariate calculus. This simplicity stems from the implicitness of the LSM, making the numerical implementation of the LSM relatively easy. The implicit formulation also means that changes in the interface topology are handled naturally. When comparing the LSM to other interface-tracking methods, such as the front-tracking method [15] where the interface is represented by piecewise continuous functions, the simplicity becomes especially clear.

The main disadvantage of the LSM, on the other hand, is that it is not a conservative method. During the course of a simulation, a fraction of fluid 1 may be converted to fluid 2 in an unphysical fashion. Various methods have been invented to circumvent this, e.g. the HCR-2 reinitialization method [16], so it is only a small effect presently. Interface-tracking methods may be conservative; an example of this is the Volume-of-Fluid (VOF) Method, but then they typically have other disadvantages. In the VOF method, for instance, the advection equation cannot easily be solved, necessitating the use of interface-reconstruction methods [17]. Recent efforts have attempted to join the LSM and VOF in order to get the benefits of both methods; this approach seems to be fairly successful [18]. In a similar spirit, recent hybrid level-set/front-tracking methods have been developed [19] that retain the implicit definition of the interface while utilizing the front-tracking method to improve mass conservation and to compute the surface-tension forces in an accurate and robust manner.

We give here the formal definition of the level-set function used in the LSM. Let Γ be the interface between two fluids, e.g. air and water, and S be the computational domain where the fluids are confined. To represent this interface, we define a *level-set function* $\phi : S \to \mathbb{R}$ with the property

$$\Gamma = \{\mathbf{x} \mid \phi(\mathbf{x}) = 0\}. \tag{1}$$

This only defines the value of ϕ at the interface Γ, and not elsewhere. The common choice here is a signed distance function. Thus ϕ is fully specified by

$$\phi(\mathbf{x}) = \begin{cases} -\text{dist}(\mathbf{x}, \Gamma) & \text{if } \mathbf{x} \text{ is inside } \Gamma, \\ \ \ \text{dist}(\mathbf{x}, \Gamma) & \text{if } \mathbf{x} \text{ is outside } \Gamma. \end{cases} \tag{2}$$

Here, the function $\text{dist}(\mathbf{x}, \Gamma)$ is the shortest distance from the point $\mathbf{x} \in S$ to the interface Γ. With this definition of the level-set function, the normal vector to the interface is given by

$$\mathbf{n} = \frac{\boldsymbol{\nabla}\phi}{|\boldsymbol{\nabla}\phi|}. \tag{3}$$

From this, the curvature is calculated by the well-known formula

$$\kappa = \boldsymbol{\nabla} \cdot \mathbf{n} = \boldsymbol{\nabla} \cdot \left(\frac{\boldsymbol{\nabla}\phi}{|\boldsymbol{\nabla}\phi|} \right). \tag{4}$$

With suitable discretizations of the derivatives involved, these quantities are easy to calculate numerically. This is often quoted as one of the nice features of the LSM, along with e.g. the very natural way the method handles topological changes [20]. In 2D, the standard discretization of the curvature is (see e.g. [21])

$$\kappa = \frac{\phi_{xx} + \phi_{yy}}{(\phi_x^2 + \phi_y^2 + \epsilon)^{1/2}} - \frac{\phi_x^2\phi_{xx} + \phi_y^2\phi_{yy} + 2\phi_x\phi_y\phi_{xy}}{(\phi_x^2 + \phi_y^2 + \epsilon)^{3/2}} \tag{5}$$

Here, e.g. ϕ_x denotes the first derivative of ϕ in x-direction, calculated using standard central differences. However, when curvature and normal vector calculations are done during a change in the interface topology, this approach fails; the error in curvature is of the order $\mathcal{O}(1/\Delta x)$ [4]. In [9], Smereka notes that "One of the major advantages of level-set methods is their ability to easily handle topological changes. However for this problem we have found this not to be the case." It is this that the present method attempts to solve.

From the defining Equation (2), ϕ is initialized at the start of a simulation. For a given velocity field $\mathbf{u}$, ϕ should be transported so that the interface follows the flow. This is done by solving the advection equation,

$$\frac{\partial \phi}{\partial t} = v|\boldsymbol{\nabla}\phi| = -\mathbf{u} \cdot \boldsymbol{\nabla}\phi. \tag{6}$$

Here v is the velocity normal to the interface, and $\mathbf{u}$ is an *extrapolated* velocity field constructed using the method in [22]. This equation is not justified here, see e.g. [23].

Solving this equation will result in transportation of the interface, but it will also degrade the accuracy of the interface representation, as ϕ is deformed from a signed distance function. To avoid this, the level-set function is periodically *reinitialized.* We follow here the PDE-based approach introduced by Sussman, Smereka and Osher [23], which consists in solving

$$\frac{\partial \phi}{\partial \tau} + \operatorname{sgn}(\phi)(|\boldsymbol{\nabla}\phi| - 1) = 0. \tag{7}$$

Here τ is a pseudo-time which is not related to the physical time in simulations. This approach is both computationally fast and accurate when used as here with a narrow-band approach. The extrapolation of the velocity field as used in Equation (6) above is performed by solving a similar type of equation. These equations are solved using pseudo-CFL numbers of 1.0 for the velocity extrapolation and 0.5 for the reinitialization. It is noted that a numerical solution of the reinitialization equation needs accurate normal vectors at the interface.

A useful property of these equations is that the characteristics originate at the interface, meaning that solving the equations numerically for N pseudo-time steps using a CFL-number of C will yield a correct signed distance function $C \cdot N$ space steps away from the interface. This has led to the use of narrow-band methods, where the level-set function and other properties such as the curvature are only calculated and used in a narrow band around the interface. This reduces the computational time significantly.

In two-phase flow simulations, the LSM is coupled with the Navier-Stokes equations,

$$\boldsymbol{\nabla} \cdot \mathbf{u} = 0, \tag{8}$$

$$\frac{\partial \mathbf{u}}{\partial t} + (\mathbf{u} \cdot \boldsymbol{\nabla})\mathbf{u} = -\frac{\boldsymbol{\nabla} p}{\rho} + \nu \boldsymbol{\nabla}^2 \mathbf{u} + \mathbf{f}. \tag{9}$$

Here $\nu = \mu/\rho$ is the kinematic viscosity, while μ is the dynamic viscosity, ρ is the density, $\mathbf{u}$ is the velocity field and p is the pressure. $\mathbf{f}$ is any external force, such as gravity, and may be zero.

These equations hold for single-phase fluid flow, but can be extended to two-phase flow using different methods. In the present work, the Ghost Fluid Method (GFM) [24] is used. This method prescribes jump conditions for e.g. the pressure across the interface based on the interface properties. The jump conditions used here are

$$[\mathbf{u}] = 0, \tag{10}$$

$$[p] = 2[\mu]\mathbf{n} \cdot \boldsymbol{\nabla}\mathbf{u} \cdot \mathbf{n} + \sigma\kappa, \tag{11}$$

$$[\mu\boldsymbol{\nabla}\mathbf{u}] = [\mu]\Big((\mathbf{n} \cdot \boldsymbol{\nabla}\mathbf{u} \cdot \mathbf{n})\mathbf{nn} + (\mathbf{n} \cdot \boldsymbol{\nabla}\mathbf{u} \cdot \mathbf{t})\mathbf{nt} \tag{12}$$

$$- (\mathbf{n} \cdot \boldsymbol{\nabla}\mathbf{u} \cdot \mathbf{t})\mathbf{tn} + (\mathbf{t} \cdot \boldsymbol{\nabla}\mathbf{u} \cdot \mathbf{t})\mathbf{tt}\Big), \tag{13}$$

$$[\boldsymbol{\nabla}p] = 0. \tag{14}$$

based on [21]. Here, $\mathbf{t}$ is the tangent vector along the interface and $[\cdot]$ denotes the jump across an interface, that is $[\mu] \equiv \mu^+ - \mu^-$. Note that $\boldsymbol{\nabla}\mathbf{u}$ and (e.g.) $\mathbf{nt}$ are rank-2 tensors. The pressure must also be decoupled from the velocity field in order to enable a numerical solution of the Navier-Stokes equations; we use here the projection method due to Chorin [25]. This gives a Poisson equation for the pressure which can be solved using freely available numerical libraries. The PETSc library is used here [26].

In the present numerical implementation, SSP-RK schemes [27, 28] are used for the time integration, while the WENO method [29] is used for the spatial discretizations. To determine the time step dynamically, we use the CFL criterion given by Kang et al. [21].

3. The Local Level-Set Extraction (LOLEX) Method

3.1. Introduction

Calculating the curvature κ of the interface between two phases is important, since it appears in the Young-Laplace formula for the capillary pressure, $\Delta p = \sigma\kappa$. Its value is used in e.g. the Ghost Fluid Method (GFM) (Equation (11)), or other methods of enforcing the jump conditions. The normal vectors to the interface are also important, e.g. when advecting the level-set function and when reinitializing it. Calculating these geometric quantities is straightforward in theory, using Equation (3) and Equation (4) to compute them from the level-set function.

However, as is often the case, in practice it is not so straightforward. The problems arise when the distance between two interfaces is of the order Δx. This is illustrated in Figure 1. The derivatives of ϕ are not defined at the kinks. As a result of this, the numerical stencils approximating the derivatives of ϕ will often produce large, erroneous values. When this happens, the curvatures and normal vectors will be erroneous. For the curvature, this error is of order $\mathcal{O}(1/\Delta x)$, which can be several orders of magnitude larger than the correct curvature value. It should be stressed that additional grid refinement does not solve this problem; e.g. for the simulation of colliding drops, one would have to continue refining the grid *ad infinitum*.

The earliest non-smearing approach to this problem, by Macklin and Lowengrub [4], uses a modification of the directional differences for points close to kinks, along with a mesh refinement for these points. The same authors introduced a curve-fitting method instead in [10], which is said to be an improvement on the directional differences and a simplification. The latter version will be referred to as the MLM (Macklin and Lowengrub Method). Further improvements to this method, and adaptations to an on-grid framework (i.e. calculating the curvature at the grid points, not at the interface), have been developed by Lervåg [12],[13]. These methods give good results in 2D, but are difficult to extend to 3D simulations due to the use of curve-fitting.

An alternative approach to the problem is due to Salac and Lu [11], and will be referred to as the Salac and Lu Method (SLM). This approach extracts separate bodies represented by the level-set function into their own, separate distance functions. Only the negative parts of the level-set function are extracted, the positive parts are reconstructed through reinitialization. This procedure removes all kinks that are caused by two or more bodies that are close to each other. For a review and comparison of the SLM, MLM and the method by Lervåg, see Lervåg and Ervik [30]. It should also be noted that the recent article by Focke and Bothe [31] discusses a similar issue, in the context of thin lamellae which form when liquid drops collide off-center. The authors introduce a method which resembles the SLM, but which also has the ability to add small amounts of liquid to the lamella region, preventing a numerical rupture.

The method considered here is a further development of the SLM. It is referred to as the local level-set extraction method, or LOLEX method in short. The reason why the SLM is insufficient in some cases, as well as the details of the present method, is given below. Suffice it to say at this point that the present method is more general, so it applies both to the cases considered by Salac and Lu and those considered by Focke and Bothe (except the stabilization of thin lamellae which the latter introduce).

Another recently presented approach is due to Trontin et al. [32], who consider a hybrid particle/level-set method. Their approach is to use the information from the tracking particles to calculate the curvature and normal vectors, with good results. This can obviously not be applied to a pure level-set method as discussed here, or e.g. a coupled level-set/VOF (CLSVOF) method as has recently become popular [18].

The previously mentioned work by Shin et al. [19] which introduces a hybrid front-tracking/level-set method is another interesting approach. The ability of their method to conserve mass globally as well as locally is impressive, and the handling of thin filaments

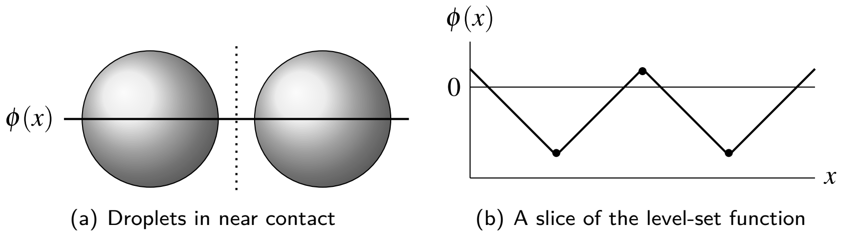
$\phi(x)$
$\phi(x)$
0
x
(a) Droplets in near contact
(b) A slice of the level-set function

Figure 1: (a) Two droplets in near contact. The dotted line marks a region where the derivative of the level-set function is not defined. (b) A one-dimensional slice of the level-set function. The dots mark points where the derivative of ϕ is not defined.

is better than the method proposed in this paper. As with the approach due to Trontin et al., this method cannot be applied to a pure level-set framework, and integrating it into an existing level-set based code would be arduous. In comparison, the method proposed in this paper can be implemented into a level-set framework with less than 500 lines of code.

An approach which has not been considered here, or by other authors in the context of level-set methods as far as we are aware, is the use of filtering. Vliet and Verbeek [33] study the estimation of curvature from a discretely sampled greyscale image, using derivative-of-Gaussian filters, and note that this outperforms a traditional curvature estimate analogous to Equation (5).

The idea of Salac and Lu, on which the present method is based, is simple when compared to the curve-fitting scheme used by Macklin and Lowengrub [4] and later by Lervåg [12, 13]. This simplicity is more in keeping with the "spirit" of the level-set method: the LSM is an implicit alternative to front-tracking methods that employ curve fitting, and this implicitness makes extending to higher dimensions straightforward. In the same fashion, the SLM is easily extensible to 3D, while the methods employing curve fitting are not. There are, however, some drawbacks to the Salac and Lu method as well.

The primary issue stems from the fact that the Salac and Lu method is aware of the global topology of the interface. A problematic area, with a kink in the level-set function close to $\phi = 0$, can be caused either by two bodies in close proximity or by a single body folding back onto itself. In the latter case, as illustrated in Figure 2, the Salac and Lu method falls back to the standard discretization, and the calculated curvature will be erroneous. This may seem like an edge case not worth considering, but simulations have shown that this often happens, e.g. when a falling droplet merges into a pool. As pointed out by Smereka [9], errors like these can be the main contribution to unphysical area loss in a simulation. Another situation where this would often be the case is in tumor simulations like those performed by Macklin and Lowengrub, as can be seen in e.g. [4, Figure 6].

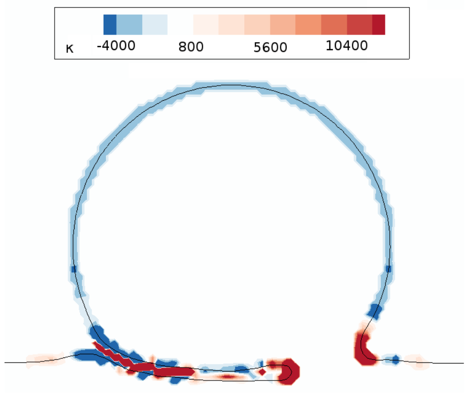

Figure 2: The curvature field plotted for the SLM. Note the red curvature field inside the air finger between the drop and the pool, which is incorrect. The color should be light blue in this area.(Figure best viewed in color.)

3.2. The idea of the LOLEX method

The method presented here tries to combine the best of the SLM with the best of the MLM. As illustrated in the previous section, the SLM is aware of the global topology of the interface, which is problematic in some cases. The MLM does not have this problem, as its curve fitting considers only the local area, but as previously stated it does not extend easily to 3D. A natural workaround to the "global awareness" is to make the Salac and Lu method consider only the local topology; say, a 10×10×10 cube around the point where we calculate the curvature.

In the following, we assume the level-set function to be located on a uniform mesh on a single CPU. The proposed method can be adapted in a straight-forward manner both into a domain-decomposition and a mesh-refinement framework. We do not discuss this in further detail here.

Since the SLM relies on reinitialization to remove kinks, a potential problem with this approach is computational efficiency, as reinitialization can be time-consuming. To avoid this problem, we want to use the standard discretization as much as possible, only resorting to the LOLEX method when we have to, i.e. when kinks in ϕ are close to the interface. To easily identify kinks, we use the quality function $Q(\mathbf{x})$ which was introduced by Macklin and Lowengrub in [4]. It is defined as

$$Q(\mathbf{x}) = \|1 - \boldsymbol{\nabla}\phi(\mathbf{x})\|_2, \tag{15}$$

i.e. the deviation of ϕ from a signed distance function, measured with the 2 norm. If $\max(\mathrm{Q}(\mathbf{x}_{\mathrm{i,j,k}})) > \eta$ for $\mathbf{x}_{i,j,k}$ in a 3×3×3 cube around the current grid point, we use the LOLEX method. A value of $\eta = 0.005$ is used here, and is seen to perform well. That is, the number of grid points where the LOLEX method is used becomes small compared to the total number of grid points. This keeps the computational cost low. The effect of varying η can be seen in Figure 10, as discussed in Section 4.2

To further decrease the computational cost, we use the "narrow band" level-set method introduced in [34]. This means that quantities such as the curvature are only calculated in a narrow band around the zero level set, where they are needed.

Having briefly presented the idea behind the present method and the scope in which it will be used, we give here a step-by-step outline of it, see Figure 3. 2D notation is used for clarity, but all steps are easily extensible to 3D. In this outline, a few arrays are introduced for storing data: `lookphi` is a copy of the global ϕ for the local area we are considering, `bodies` indicates the bodies present using increasing integers, and `locphi` holds the local ϕs that are extracted from the global ϕ and then refined into more accurate representations of the local bodies present. The quantities `ilmax`, `jlmax` and `klmax` represent the number of grid points, in the x, y and z directions respectively, of the *local* grid. The values of `ilmax`, `jlmax`, `klmax` are all set to 7 in the simulations performed here. Their values are independent of the global grid size. Sensible values of these are between 5 and 11; since they must be odd, smaller than 5 gives too low resolution, and larger than 11 starts eliminating the advantage of using a localized method. The value of 7 used here gives good results, and increasing it to 9 gives only a small change while increasing the computational cost. In the limit `ilmax` $\to$ `imax` etc. the method of Salac and Lu is recovered.

The steps in the algorithm that warrant further comments are: identifying the bodies present, explicitly reconstructing the signed distance, extrapolating to the ghost cells, and reinitializing. These will be considered further in the next section and subsections.

```
↪ Loop over the computational domain using indices i,j.
↪ If ($\mathbf{x}_{i,j}$ not close to interface) do nothing. A point is defined as close to an interface
  if all $\phi(\mathbf{x}_{n,m})$ for $(n,m) \in [i-1,i+1] \times [j-1,j+1]$ is either negative or positive.
↪ Else if ( $Q(\mathbf{x}_{n,m}) \leq \eta \ \forall (n,m) \in [i-1,i+1] \times [j-1,j+1]$ ) use ordinary method.
↪ Else use LOLEX method:
    ↪ Copy $\phi$ in a [-1,ilmax+2]*[-1,jlmax+2] square around i,j into the
      lookphi array.
    ↪ Identify the bodies present in the [0,ilmax+1]*[0,jlmax+1] square, store
      this in the bodies array.
    ↪ For each body, extract the relevant part of the lookphi array into
      locphi(:,:,bodyno). This array has 3 ghost cells on the boundary out-
      side ilmax*jlmax; these are not used until the extrapolation further down.
      Extracting means:
        – copying lookphi for the internal points of *this* body
        – copying lookphi for external points that are not next to more than one
          body
        – explicitly reconstructing the signed distance for external points that are
          next to more than one body
        – setting a value of 2*dx for all other points
    ↪ Once the locphi array has been filled for all bodies, the values are extra-
      polated into the ghost cells. The extrapolation is zeroth-order, as will be
      explained further down.
    ↪ The locphi array is then reinitialized for all bodies. This erases the problem-
      atic kink, as well as the value of 2*dx which was set previously. Thus this
      value is unimportant, as long as it is $> 0$.
    ↪ Using these local $\phi$'s, the curvature and normal vectors can be calculated
      for each body. The curvature and normal vectors corresponding to the body
      which is closest to the current grid point are used.
```

Figure 3: A step-by-step outline of the LOLEX algorithm.

3.3. Details of the method

Some steps of the algorithm outlined need further explanations. This is either because they are too technical to be fully described in the previous short outline, or because they have not been properly motivated yet. The steps that will be considered are identifying the bodies present (Section 3.3.1), explicitly reconstructing the signed distance (Section 3.3.2), extrapolating to the ghost cells (Section 3.3.3), and reinitializing (Section 3.3.4).

3.3.1. Identifying the bodies present

To identify the bodies present, a recursive routine is used, which starts at a seed point in a body and iterates through the entire body, marking it as a body in the `bodies` array. The seed point is found by scanning the computational domain for points with $\phi < 0$. The recursive routine is called `bodyscan` here. The `bodies` array starts with a value of `unchecked`, and bodies found are marked using increasing integers. The recursive subroutine will have marked the entire first body when its first call returns.

A final point to note about the routine given here is that even though a recursive subroutine is used, memory usage will not be problematic. This is because the routine operates on a small array whose size is independent of the grid size. In 3 dimensions and with the presently used size of the local area, the array `bodyscan` would have `11*11*11` = 1331 elements. This routine can maximally be called 1331 times, giving a worst-case memory consumption of 13.5 MB. In reality this number would typically be less than half of that. This will not cause memory problems, although it is too large to fit in the CPU cache for some processors. The performance impact has not been tested here, as the 3D calculations are only considered as a proof-of-concept, and have not been optimized for speed. In 2D the memory use is naturally much smaller.

3.3.2. Explicit reconstruction of the signed distance

For some points with $\phi > 0$, two or more bodies are within Δx of the point. This means that the value of ϕ is probably incorrect, since it has to be the distance to two separate bodies at the same time. We will call such points "dependent points". These points are found using the `bodies` array: if this array has more than one unique positive integer value in the four points adjacent to the present point, it is dependent. Because ϕ is likely incorrect for dependent points, we discard its value, and instead explicitly reconstruct the distance to the relevant interface. The procedure used is due to Adalsteinsson et al. [35].

When we consider such a dependent point, it lies right next to two interfaces. When reconstructing the distance, only one interface is of interest, so the other one is momentarily removed. Note that the signed distance is always positive for exterior points, so it is just the normal distance.

The procedure in [35] is as follows. The point (i, j) which we are considering is next to the interface of current interest. We ignore all other interfaces. Up to rotational symmetry, there are four possible cases. An illustration of these cases can be seen in Figure 4.

We examine the four cases (**a** to **d**) more closely:

a The interface crosses one of the lines from (i, j) to its four neighbors. In this case, we use the distance to the interface along this line as our distance. This distance is

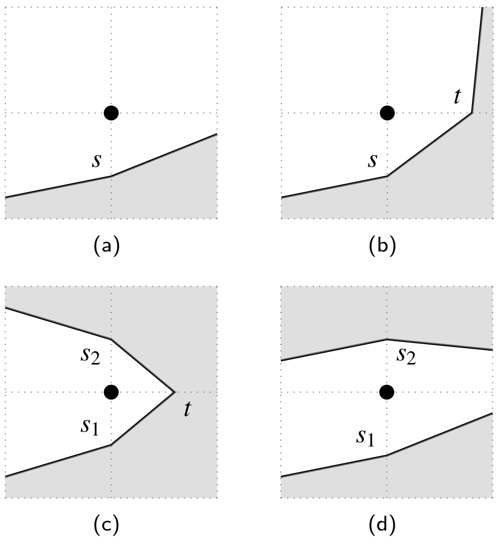

Figure 4: Cases for the neighborhood of a point.

given by

$$s = \Delta y + \phi(i, j-1) \tag{16}$$

where we have assumed that $(i, j-1)$ is the neighbor on the other side of the interface. Since this neighbor is an internal point, it has $\phi < 0$. The distance to the interface is the distance to the neighboring grid point (Δy) minus the distance from that grid point to the interface, which gives this formula. It is best to use only the ϕ-value inside the body, since it is less likely to be distorted.

b The interface crosses two of the lines, and these two lines make out a corner of the 2×2 grid around (i, j). In this case we use the shortest distance to the straight line between the two points of intersection. The distance d is given by the formula

$$\left(\frac{d}{s}\right)^2 + \left(\frac{d}{t}\right)^2 = 1. \tag{17}$$

As long as $s^2 + t^2 \neq 0$ this equation can be solved, and the positive solution is

$$d = \frac{st}{\sqrt{s^2+t^2}} \quad . \tag{18}$$

If we have $s^2 + t^2 = 0$, then $s = t = 0$, so it is obvious that the distance to the interface is $d = 0$.

c The interface crosses three lines. We construct the two straight lines between the points of intersection, and use the shortest distance to either of these two lines, given by

$$\left(\frac{d}{\min(s1, s2)}\right)^2 + \left(\frac{d}{t}\right)^2 = 1. \tag{19}$$

d The interface crosses two lines. These lines are on opposite sides of the point (i, j). In this case, we use the shortest of the two distances, so $d = \min(s1, s2)$.

These formulae can be extended to three dimensions, where the possible cases are more numerous. In 3D, the central point has two additional neighbors. This means there are more variations in addition to the cases considered above. This is not considered in detail here.

3.3.3. Extrapolation

After the interior of the `locphi` array has been filled, the ghost cells must be filled before we can reinitialize the local ϕ. Two ways of doing this are illustrated in Figure 5. A first approach is to use linear extrapolation, which should work well since ϕ is a linear function in 1D. However, it turns out that this does not work. A fundamental property of the reinitialization equation (7) is that its characteristics originate at the interface $\phi = 0$. This is why the present method (and the SLM) works – we only need a few cells directly next to the interface to have the correct value of ϕ, and reinitialization will fix the rest. It also means that reinitialization will never move the position of the interface, which is a desirable property in general.

The problem with linear extrapolation occurs when we extrapolate starting on the opposite side of the kink from the interface. In this case, the values of the local ϕ are tending towards 0 from above, which means that extrapolation can reintroduce the other body (which we removed in the first place). When this happens, reinitialization cannot fix the values beyond the kink, since it cannot move the interface reintroduced by extrapolation. A straightforward alternative is to use a zeroth-order extrapolation. This means simply copying the values along the edges into the ghost cells. It is obvious that this will never cross $\phi = 0$, so reinitialization works as intended.

The difference between these two is shown in Figure 5. In (a), a zoom in on the global level set of a droplet touching a pool is shown. In (b), the local level set of the lower body (the pool) is shown after extraction and explicit reconstruction. Here, the values on the edges are not set, indicated in grey. In (c), the same is shown after first-order extrapolation, and in (d) after zeroth-order extrapolation. In (e), the first-order extrapolated ϕ is shown reinitialized, and in (f) the zeroth-order extrapolated ϕ is shown reinitialized. Note in particular that in (e), a kink still exists after the entire procedure (green line), so the geometric quantities calculated would still be wrong if the derivatives cross the kink.

The corner cells on the boundaries must also be set. Here, these all get the value from the corresponding corner of the internal grid.

3.3.4. Reinitialization

When the extracted local level-set has been extrapolated, it must then be reinitialized before the geometric quantities are calculated. This is essential in order to have good values of the level-set function outside the interface. The entire LOLEX method hinges on the fact that reinitialization restores the local level-set to a signed distance function, so that ordinary discretizations will not give errors. This is not entirely straightforward, however.

When reinitializing, we require at least some points on either side of the interface with decent ϕ-values, i.e. ϕ being the signed distance to the interface. In addition to this, we

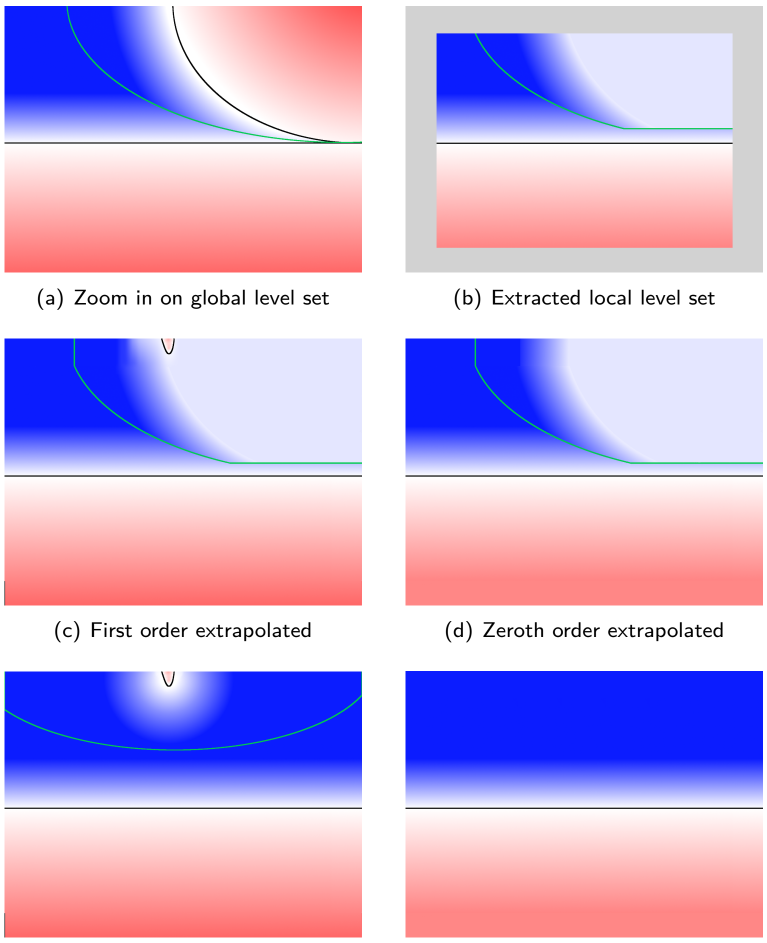
(a) Zoom in on global level set

(b) Extracted local level set

(c) First order extrapolated

(d) Zeroth order extrapolated

(e) First order, reinitialized

(f) Zeroth order, reinitialized

Figure 5: Extraction, extrapolation and reinitialization of the local level set is shown, for the lower body in Figure (a). Red indicates a negative value, blue a positive value, and white indicates zero. The green lines indicate kinks in the level set function, and the black lines are the zero level sets. A detailed explanation of the figures is given in Section 3.3.3. (Figure best viewed in color.)

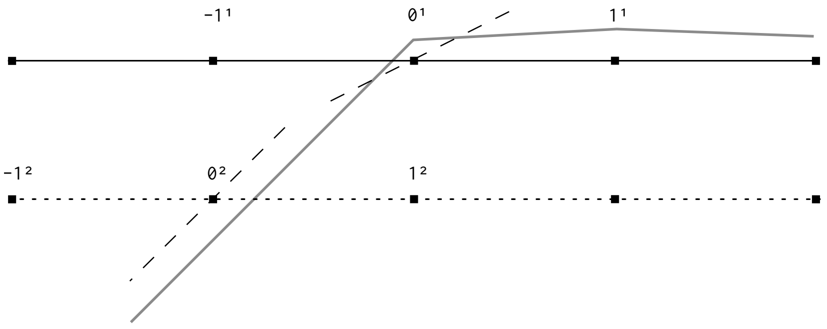

Figure 6: Why we reinitialize from a lower level set: At the lower level set, indicated by the dotted line, values of e.g. $\boldsymbol{\nabla}\phi$ are more accurate at the grid point which is closest to the grey line than for the zero level set. The grey line indicates the local level-set function ϕ. The dashed lines indicate $\boldsymbol{\nabla}\phi$ calculated using central differences.

need to know the smeared sign function, and most crucially, the normal vectors at the interface. Thus we are faced with a bootstrapping problem: accurate normal vectors are required in order to accurately calculate the normal vectors. This is only a problem when the global interfaces are very close; when there is a moderate distance (i.e. more than one grid point between the interfaces), the normal vectors can be calculated at the interface using the local level-set.

The solution to this conundrum is to exploit the redundant information which is stored in the level-set function. To illustrate this redundancy, imagine that you are walking along a normal vector to the interface. At each grid point you pass, you are told the current distance to the interface. As long as you do not pass any kinks, this information is redundant: using the value at the first grid point you pass, you can calculate the value at the next grid point, and the one after that, given that you know the grid spacing.

What this means for the present case is that we have information inside the current body that we can use. Most importantly, we can calculate the normal vectors without problem for internal points. This means that we can reinitialize a level set different from $\phi = 0$, e.g. $\phi = -0.8\Delta x$, and get essentially the correct ϕ afterwards. We are not guaranteed to get exactly the correct ϕ, but as we cannot obtain the correct ϕ anyway, we will settle for a good approximation. An illustration of this in 1D is shown in Figure 6, where the extracted local level-set function ϕ is shown in grey. Note that e.g. the value of $\boldsymbol{\nabla}\phi$ at the grid point $\mathtt{0}^2$, shown with a dashed line, is much closer to 1 than the value at the grid point $\mathtt{0}^1$. When the lower level set is used, we momentarily move the interface further to the left in this figure, so the grid point $\mathtt{0}^2$ is closest to the interface. It is obvious that we have a better chance of restoring a signed distance function with the correct location of the interface if we reinitialize from the lower level set.

The value of $-0.8\Delta x$ used here gives the most accurate results. If the value is too close to zero, the benefit of reinitializing from a lower level set is reduced. However, if the value is too large, we risk having this lower level set too close to the edges of the local domain, and we increase the potential error caused by reinitializing from a different level than zero. The optimal result is afforded by choosing a value somewhat below

Table 1: Parameters used in the LOLEX method, along with values used and sensible ranges.

Parameter	Value	Sensible range
Local grid size	7	5–11
Gradient threshold η	0.005	0.01–0.001
Reinit. level set	$-0.8\Delta x$	$-1.0\Delta x$ to $-0.5\Delta x$

$-0.5\Delta x$, since this ensures that the grid point $\texttt{0}^2$ is always closest to the interface, while minimizing errors from the edges of the domain.

Another problem solved by this is the fact that the values directly outside the zero level set may be incorrect in some cases. In particular, this happens when an outside grid cell is not flagged as dependent, but its value of ϕ still deviates from that dictated by a signed distance function. Tests have shown that this sometimes occurs, and that it distorts the reconstructed local level set.

Reinitializing from a different level may sound somewhat complicated to do, but the implicit formulation springs to the rescue again. To reinitialize from a lower level set, we simply add a positive constant to ϕ at every local grid point, call the reinitialization routine on this ϕ, and then subtract the same constant from the reinitialized ϕ. The effect of this is illustrated in Figure 7, which is an extreme case. Here, reinitialization of two very close bodies (concentric circles) has distorted the global level-set function close to and outside the interfaces. The reinitialized local level-set function is also wrong, but the one which is reinitialized from a lower level set gives a much smoother representation of the interface, which agrees with the contour lines further into the body. This smoother representation will, in turn, give a significantly more accurate curvature. A plot of the curvature calculated with and without this improvement is shown in Figure 8 for the concentric circles case; this global interface configuration can also be seen in Figure 11 further down. This plot shows the curvature along the inner circle. It is seen that the improvement is large, particularly in this case when two interfaces are close. The curvature calculated using the standard method is not shown, as it is outside the y-axis range in this figure.

While the curvature calculated using the LOLEX method is close to the analytical value, there is still a more or less constant error of 1–2%. It turns out that this error is caused by the reinitialization of the local level set, as is indicated in this figure as well. The line captioned ‘Forced LOLEX’ shows the LOLEX method used on a single interface corresponding to the inner circle. Here, the level-set function is correct and the standard method gives an error for the single interface which is smaller than the line width in this figure. When we force the use of the LOLEX method, the only difference from the standard method is the extrapolation and reinitialization, meaning that these must be the culprits. To mitigate this, a more accurate reinitialization procedure could be used, e.g. the HCR method due to Hartmann et al. [16].

3.3.5. Parameters of the method

In the LOLEX method as presented here, there are a number of parameters that can be varied. An overview of these is given here, along with the values used presently, and sensible ranges, in Table 1.

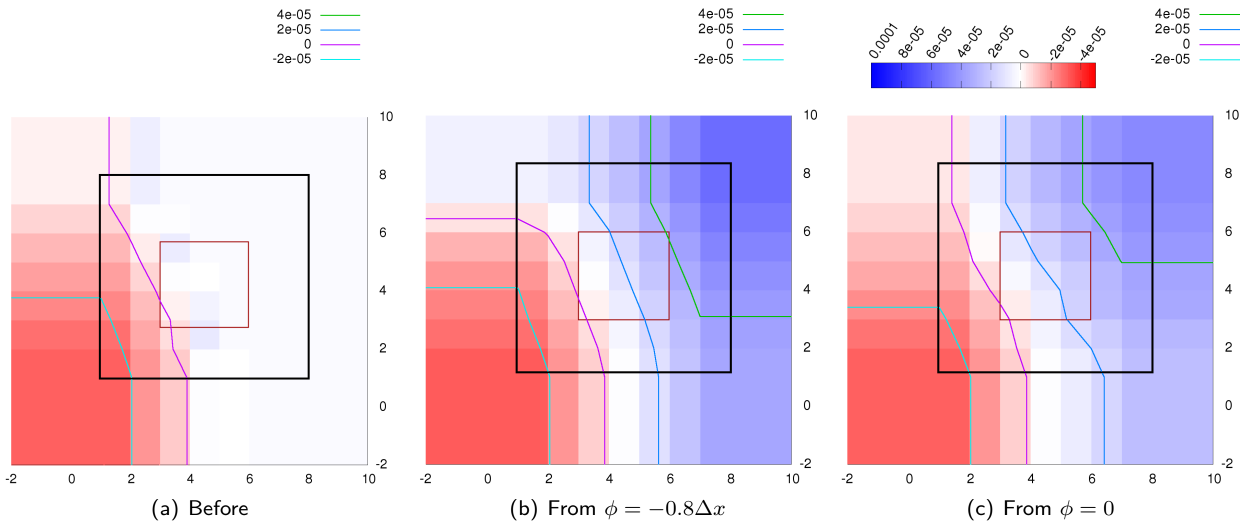

Figure 7: The LOLEX method on a global level set which is distorted due to reinitialization of very close bodies. The global bodies are two concentric circles. (a) Local ϕ before reinitialization. (b) Local ϕ reinitialized from $\phi = -0.8\Delta x$. (c) Local ϕ reinitialized from $\phi = 0.0$. The black square indicates the boundary to the ghost cells, and the red square indicates the $3{\times}3$ central points that are used in the final curvature calculation.

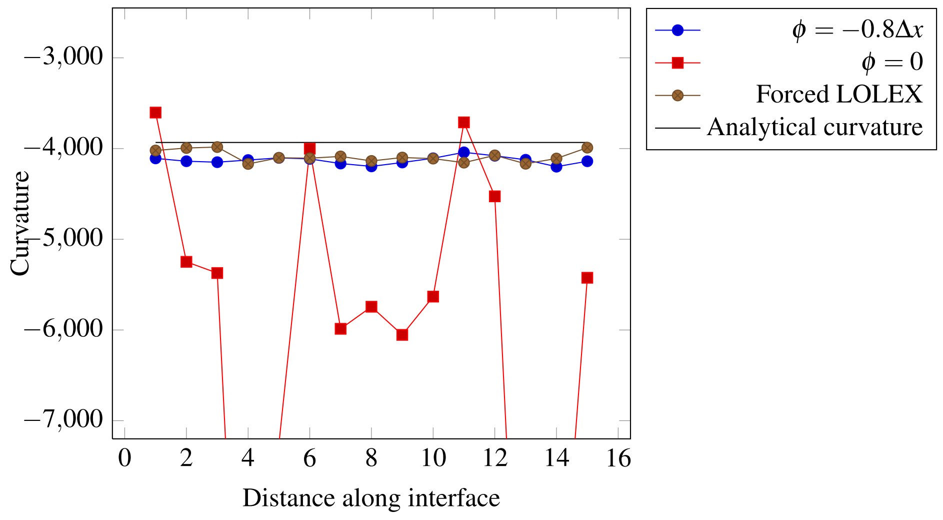

Figure 8: Lineplots of the curvature along the interface when reinitializing from both the zero level set and a lower level set. Also shown are the curvature calculated when forcing use of the LOLEX method on a single interface, and the analytical curvature.

After the local level sets have been extracted correctly, the standard discretizations can be used to calculate the normal vector and curvature. As the curvature and normal vector cannot be multiply defined at a single grid point, we must combine the information from different local level sets. To do this, we simply select the one corresponding to the interface which is closest to the central point.

As the present method uses reinitialization on a local grid for each grid point where it is used, the performance impact of the method could become large. To avoid this, the quality function $Q(\mathbf{x})$ is used to restrict the use of the method. In a typical falling drop simulation, the present method will only be used in a small percentage of the total number of time steps, and even then, it will typically not be used for all points along the interface. This means the computational cost of the present method has a low impact on the total runtime of a simulation. We note that the computational cost is lower than in the method of Salac and Lu, since that applies reinitialization to the entirety of the bodies present.

3.4. Summary

In this section the presently used LOLEX method has been described in detail. The method is used for grid points where the level-set function deviates from being a signed distance function, where it extracts one or more local level sets, removes any kinks in these by use of reinitialization, and finally uses these local level sets to calculate the curvature and normal vectors. The values corresponding to the interface which is closest to the current grid point is used.

The method is motivated in that it is more general than the previous method by Salac and Lu [11], handling bodies which fold back onto themselves, and it extends more easily to 3D than the previous methods by Macklin and Lowengrub [4, 10] and by Lervåg [12, 13], which use curve-fitting schemes. The parameters of the method are given in Table 1. Results, both for static and dynamic simulations, are given in the next sections.

4. Geometric results

In order to test the LOLEX method, some static interface configurations were used that replicate typical situations occurring in simulations of droplet collisions.

4.1. Circles and straight interfaces

The first test case consists of three circles and a straight-lined interface, where two of the circles and the straight-lined interface are joined together. The results for this case are shown in Figure 9 for the LOLEX method, the SLM, and the standard method. In this figure, the interfaces are shown as black lines, and the color indicates the curvature. The background curvature of 0 is indicated in white, blue indicates a negative curvature and red indicates a positive curvature. The figure illustrates that the standard method produces positive unphysical curvatures several places, both between the circles and the straight interface and between circles. The Salac and Lu method remediates the situation somewhat, but still has problems where the circle folds back onto the straight interface, and at the bottom of the middle circle, which is particularly close to the straight interface. The LOLEX method produces positive curvatures only where they are expected and needed.

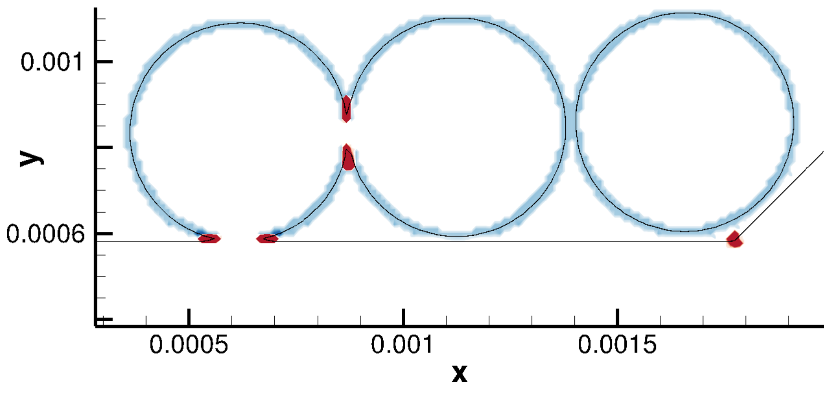

(a) LOLEX method

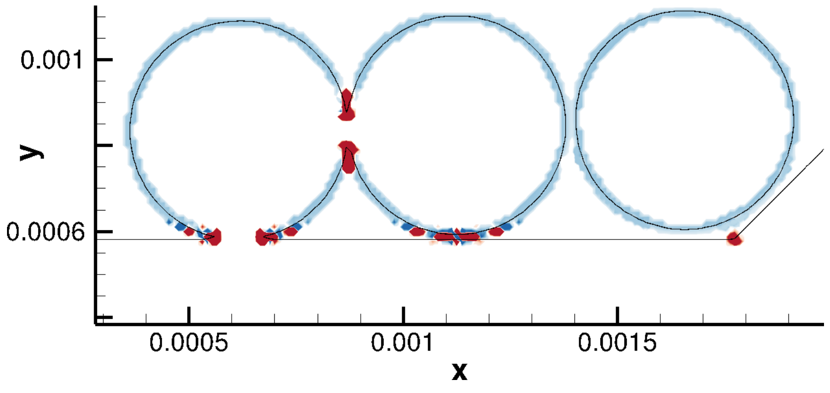

(b) Salac and Lu method

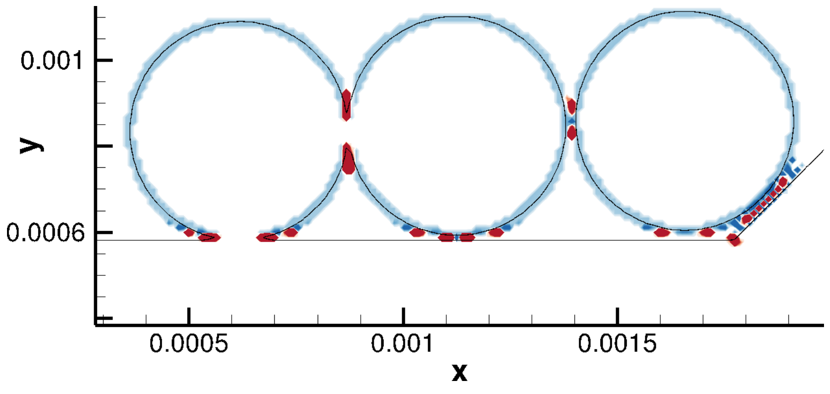

(c) Standard method

Figure 9: Comparison of curvature calculation methods for circles and straight interfaces. The color indicates the curvature; white is zero, blue is negative and red is positive.

4.2. Droplet falling onto a pool

In order to compare the behavior of the LOLEX and the standard method for different interface separations, a test case was considered which mimics a droplet falling onto a pool. In this case, a 0.2 m diameter circle and a horizontal line were initialized in a 1m $\times$1m domain. The separation between the circle and the line was varied from $3.6\Delta x$ down to $0\Delta x$ in increments of $0.1\Delta x$. For each separation, the curvature was calculated at all points within the narrow band close to the interfaces, and the supremum-norm $\|\kappa\|_\infty$ of the curvature values was calculated. This was done using the standard and the LOLEX method, for grid resolutions of 64$\times$64, 256$\times$256 and 1024$\times$1024. The analytical curvature is 10 for the circle and 0 for the line, so the supremum norm should be close to 10. The results are shown in Figure 10.

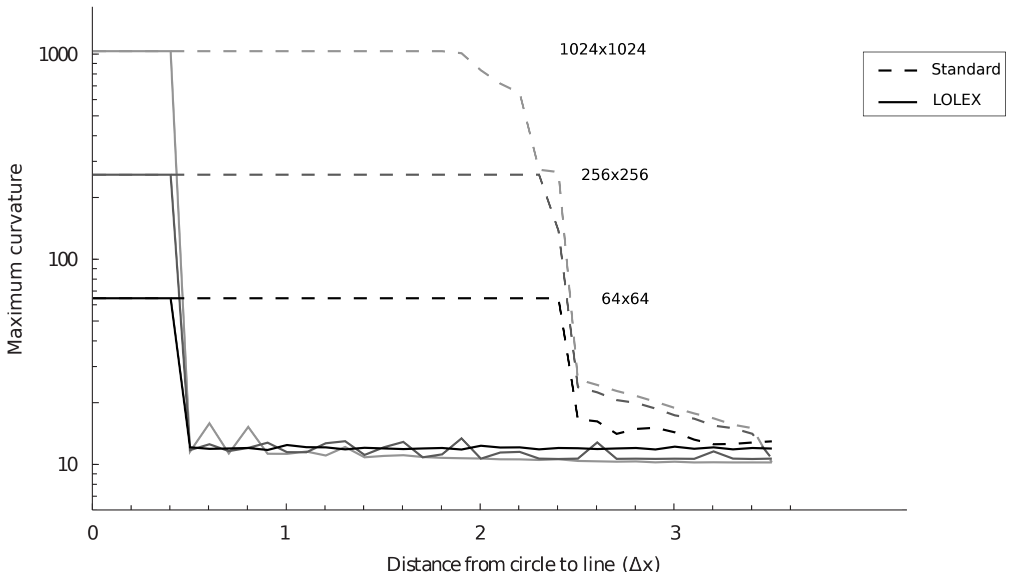

Figure 10: Supremum norm of the curvature for decreasing interface separation. Dashed lines: results using the standard method. Solid lines: results using the LOLEX method. The lines are shaded lighter with increasing grid resolution. The analytical curvature of the circle is 10.

As is seen in this figure, the standard method returns the value used in regularizing the curvature, $\|\kappa\|_\infty = \frac{1}{\Delta x}$, when the interface separation becomes smaller than about 2.4 Δx. Increasing the grid resolution does not improve the situation. Note that the y axis in this plot is logarithmic. Meanwhile, the LOLEX method gives decent values close to the analytical value of 10 all the way up to when the interfaces merge, which happens at a separation of 0.2 Δx. It is seen that the small deviations for the LOLEX method are reduced when the grid resolution is increased.

A final thing which may be illustrated using this figure is the effect of the parameter η. This parameter indicates how much the level-set function ϕ has to deviate from being a signed distance function before we switch from using the standard method to the LOLEX method. In the circle-line case in Figure 10 the value of $\eta = 0.005$ (used throughout this paper) triggers the switch for the first point when the distance is $4.2\Delta x$. Using $\eta = 0.01$

as in [10], the switch is made at $3.9\Delta x$. Both these distances are in the region where the standard method gives good answers, so the LOLEX method is not very sensitive to the precise value of η as long as it is in this range.

In addition to the curvature, accurate normal vectors close to the interface are desirable in level-set simulations. The importance in reinitialization has been suggested above, coming from the fact that normal vectors are used in finding the upwind direction. Normal vectors are equally important in calculating the extension velocity, where an error would lead to the interface not moving according to the flow.

4.3. Concentric circles

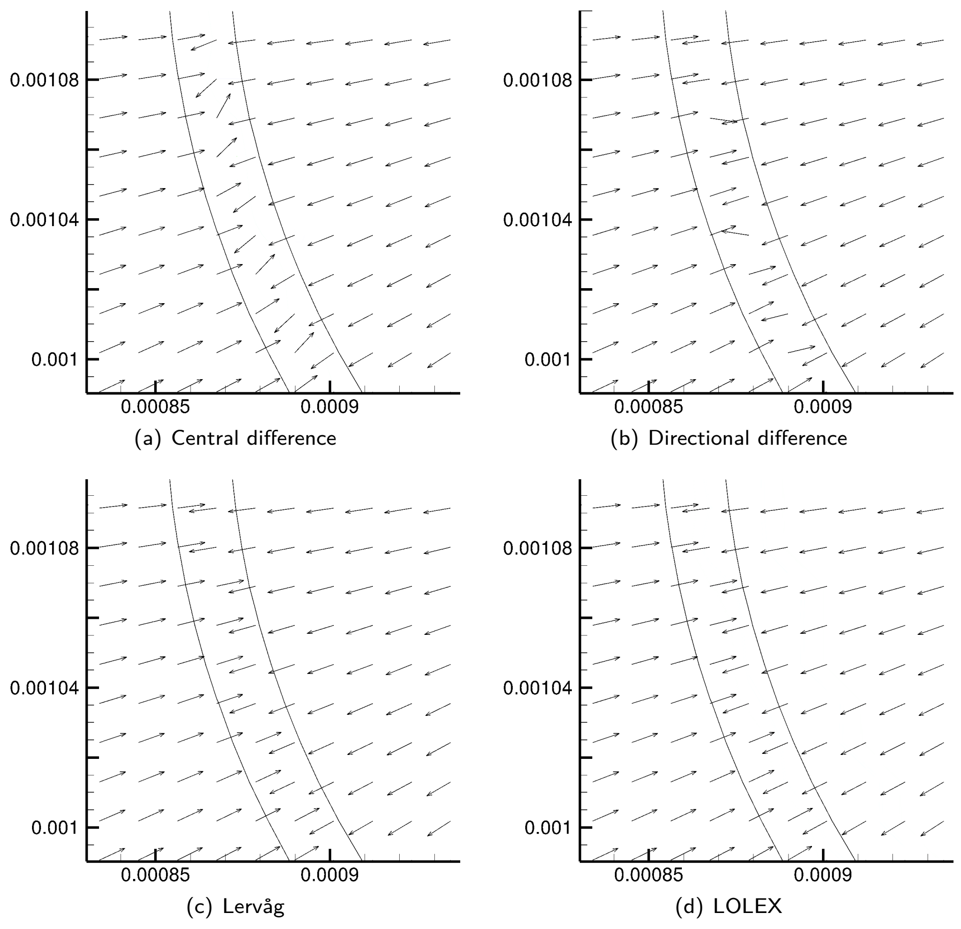

Figure 11: Comparison of normal vector calculations using different methods.

In order to compare the proposed method to the standard method, a geometric test case was considered which replicates the demands of simulating merging interfaces. The calculated normal vectors are compared both to the standard central-differences discretization, to a directional-differences discretization as described in [4], and to the curve-fitting method of Lervåg [13].

In this test case, two concentric circles were initialized, as if we had a thin ring of fluid 1 inside fluid 2. The width of this ring was $1.6\Delta x$. This test case is interesting, since it reveals grid effects or anisotropies. It also replicates the situation of a thin film that forms between a droplet and a pool for cases where the droplet deforms the pool surface before merging. This has been observed experimentally, see e.g. [36]. The results for all four methods are shown in Figure 11.

In this figure it is seen that the directional difference method is not much better than the central difference method. This is partly what prompted the use of curve fitting methods; Macklin and Lowengrub initially used directional differences and additional grid refinement in [4], but switched to curve-fitting methods in [10]. As is seen in Figure 11 (c), curve fitting methods (the method by Lervåg is used here) give the correct result. In (d), we see that the LOLEX method also gives the correct result. It is impossible to distinguish the results in (c) and (d) without overlaying the figures and zooming in a lot. We calculated the maximum RMS deviation between the LOLEX method and the other three methods compared in Figure 11, e.g. $\|\sqrt{(n_x(d) - n_x(a))^2 + (n_y(d) - n_y(a))^2}\|_\infty$. This was 0.0086 for the Lervåg method, 0.92 for the Central difference and 1.78 for the Directional difference; a 90° difference would give $\sqrt{2}$. We note that the maximum error is largest for the Directional difference, while the average error is largest for the Central difference. The difference between the LOLEX and Lervåg methods is too small to have any impact on the simulation results.

As pointed out several times already, the main advantage of the present LOLEX method over methods employing curve fitting is that it scales easily to 3D. This is because the present method retains the implicitness of the level-set method. A 3D extension of the Macklin and Lowengrub method, on the other hand, would fit a local surface to the point of interest, as they indicate in [10]. Curvature estimation in 3D based on local surface fitting has long been a topic of research in computer vision, see [37] for a review of various methods including the use biquadratic surfaces and of splines. The conclusion of [37] is that these methods are very sensitive to numerical noise (in their context, sensor noise). In the current case, noise is to be expected, as can be seen in Figure 7 (b). Due to this fact, methods in computer vision that avoid local surface fitting and calculate only the sign of the curvature have been introduced, since this quantity can be calculated more reliably[38]. This is not a viable alternative in two-phase flow simulations as considered here.

4.4. 3D bubble above a plane

A curvature calculation using the LOLEX method on a 3D case is shown in Figure 12. In this case, a bubble is placed above a plane, with distance $1.2\ \Delta x$ at the closest. The grid is $50\times50\times50$, and the bubble radius is $12.5\ \Delta x$. The surfaces are colored according to the curvature (interpolated to the surface). In Figure 12 (a), the standard method is used. In 3D, this is the 27-point stencil given by Kang et al. [21]. In Figure 12 (b), the LOLEX method is used to extract the local level sets, and the curvature is then calculated using the same 27-point stencil on these local level sets. It is seen that the LOLEX method performs much better than the standard discretization in areas where the bubble and plane are in close proximity. Note that the plane is not shown here, only the bubble. The kink in the global ϕ is below the bubble.

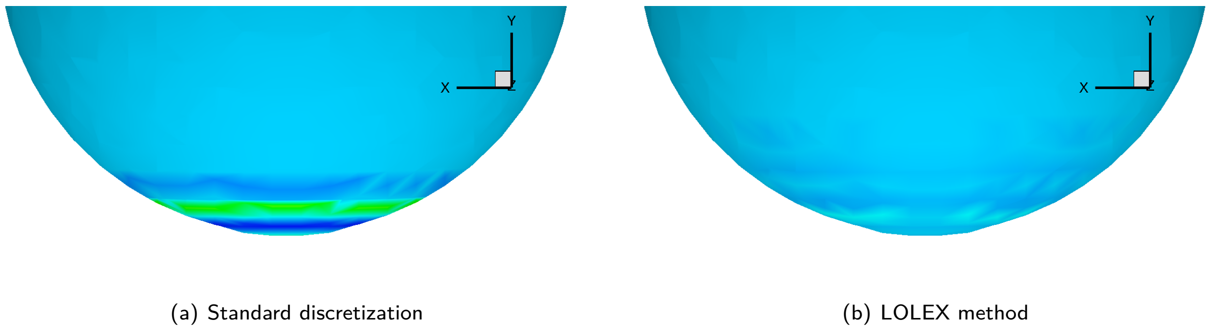

Figure 12: 3D bubble above a plane (not shown). Comparison of the standard curvature discretization (a) and the LOLEX method (b). The surfaces are colored according to the curvature, and the standard method is seen to give large errors close to the kink in the level-set function (which is below the sphere), seen as green and dark blue bands.

Comparing to the analytical curvature, which in this case is -10 for the spherical bubble, it is seen that the standard discretization performs well away from kinks, where the variation in curvature is at most $\pm0.2\%$. Close to the kink, the standard discretization has errors of $\pm80\%$, seen as green and dark blue bands in Figure 12 (a). The LOLEX method has the same variation as the standard method away from kinks, while the variation is $\pm2\%$ close to the kink, seen as light blue spots in Figure 12 (b). Thus it is seen that the LOLEX method gives an error which is an order of magnitude lower than the standard method close to kinks in the level-set function. There is still a small error of the same size as reported above in 2D, which is again probably caused by reinitialization. A deviation of this magnitude is unlikely to have a large impact on simulations, in contrast to the errors from the standard discretization.

To the knowledge of the authors, improved calculation of geometric quantities for a pure level-set formulation in three spatial dimensions that handles general topologies have not been reported before in the literature. Salac and Lu report results of 3D simulations in [11], but it is not known how (or if) they handle problems like that illustrated in Figure 2, i.e. a body folding back onto itself. They also do not discuss the problem of needing good normal vectors at the interface in order to solve the reinitialization equation.

Given the current state of developments toward petascale supercomputers, and particularly the rapid evolution in GPU-accelerated solvers, dynamic 3D level-set simulations of colliding bodies are going to become more and more common. As this happens, a method such as the present one will be necessary in order to get trustworthy results for situations where accurate curvature is important.

5. Dynamic results

As discussed previously, the case of a single droplet of liquid falling onto a pool of the same liquid, either through gas or another liquid, has been widely studied. Thus it is a good benchmark on which to test the proposed method, since detailed experimental results are available.

When considering this case, the main dichotomy is between a droplet falling through gas and a droplet falling through liquid. We will consider both cases here, since both are interesting from an industry standpoint. These two cases present different challenges to numerical simulations. The liquid-in-gas case has a high density difference between the two fluids, which is known to be a difficult case. Sussman et al. have studied this problem, and have produced good results using a hybrid LSM-VOF method [18]. The liquid-in-liquid case, on the other hand, can be time-consuming to simulate due to the viscous term in the CFL-criterion used here [21], but is not challenging with respect to density differences.

5.1. Decane droplet in water merging with decane pool

The simulation discussed here consider two immiscible liquids, where a droplet of the heaviest liquid is placed in the lightest liquid above a pool of the heaviest liquid. In the experimental work by Chen et al. [39], the droplet is made to rest on the pool, and then merging happens after some time. The heavy liquid is water, and the light liquid is a mix of 20 % polybutene in decane. The droplet diameter is 1.1 mm. As the droplet and interface are brought into proximity, a thin film is formed between them. This thin film drains, and after some time the film ruptures and the droplet merges with the interface. In the Chen et al. experiments, the merging happens at the central point, but off-center merging has also been reported for larger droplets [40].

A simulation was performed with the same fluid properties and droplet dimension as reported by Chen et al. The computational domain was 6×6 mm, the grid was 400×400, and the CFL-number was 0.8. The results are shown in Figure 13. The agreement between the simulation and experimental results is very good.

In this simulation, the point of merging is decided mainly by grid effects when the droplet deforms the interface forming a thin film. With the present method, we must simply hope that precisely what happens at the time of merging does not significantly affect the following behaviour. Comparing Figure 13 (a) and (b) indicates that in this case the precise mechanisms of merging are not very important, as the numerical and experimental results agree very nicely. To accurately capture the thin film behaviour, the grid resolution would have to be extremely fine. Hodgson and Lee [41] report that the width of the thin film between a droplet and a pool for the water-toluene system they study is four orders of magnitude smaller than the droplet diameter, i.e. around 100 nanometers. It is possible that an adaptive grid could be able to resolve such a thin film, but since there is no analog to the Knudsen number for liquids, it is not immediately clear whether the continuum description of the Navier-Stokes equations still holds at this length scale.

Comparing the LOLEX method and the standard method on this case, the standard method gives a more oscillatory pressure field around the contact point, as seen in Figure 14. This increased pressure inside the thin film delays the rupture of the film, seen as a slightly increased width of the film in Figure 14 (b).

5.2. Water droplet falling through air onto a water pool

Considering the case of a liquid in gas, a simulation was performed of a 0.18 mm diameter water droplet falling through air at 0.29 m/s and impacting a deep pool of water. Experimental results for this case due to Zhao, Brunsvold and Munkejord are found in

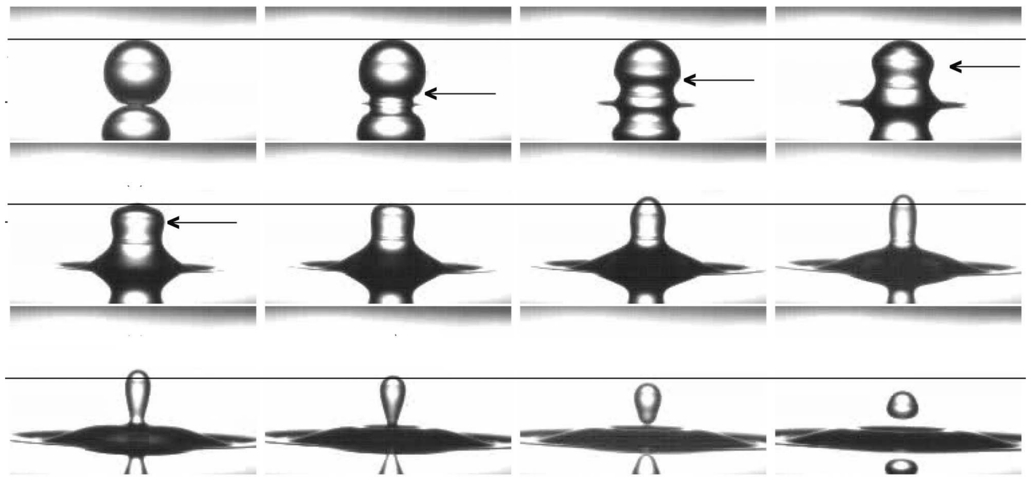

(a) Experimental result

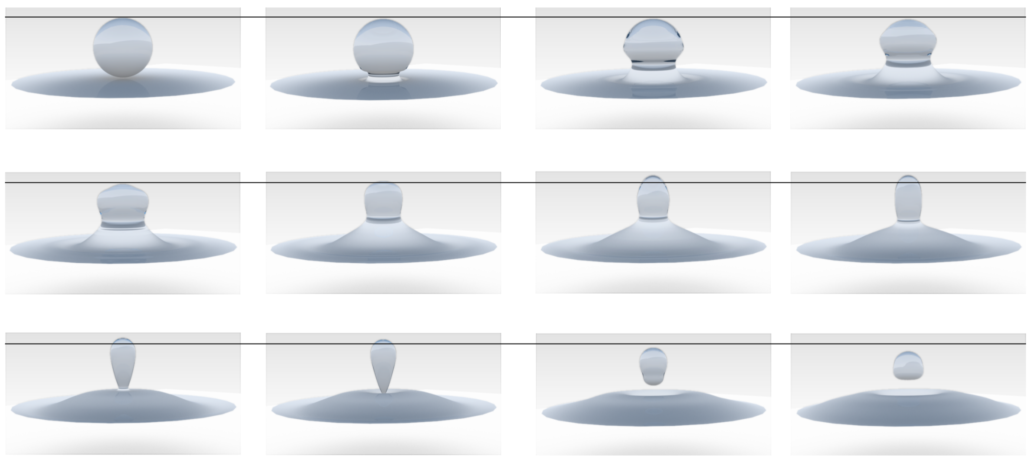

(b) Simulation result

Figure 13: A 1.1 mm diameter water droplet merging with a water pool. The ambient fluid is 20% polybutene in decane. Snapshots are taken 542 μs apart, the arrow indicates the capillary wave, and the horizontal lines indicate the top of the bubble in the first frame. Figure (a) is the experimental result, reprinted with permission from [39], copyright 2006 American Institute of Physics. Figure (b) is the simulation result.

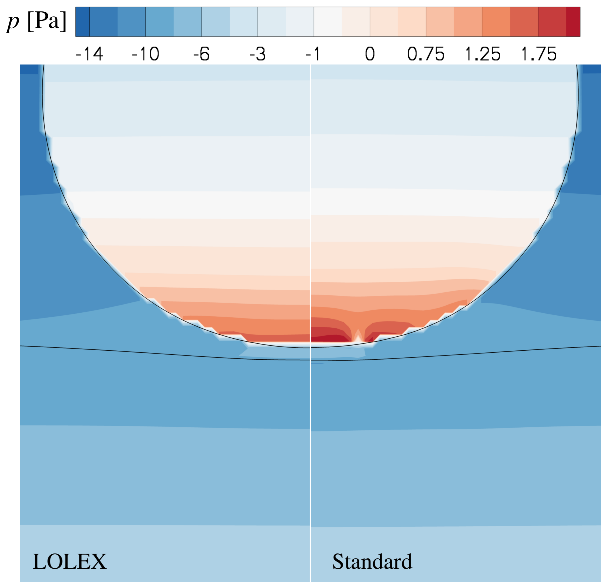

Figure 14: Water droplet in a mixture of polybutene and decane, about to merge with a water pool. Comparison of the pressure field using the LOLEX method and the standard method at $t = 0.007$ s.

[42]. These results indicate that a partial coalescence occurs, but the high-speed camera used was not fast enough to capture all the details of the partial coalescence process.

The simulation was performed using axisymmetry. The computational domain was 0.7 mm $\times$ 0.7 mm, resolved using a 401$\times$401 Cartesian grid. The CFL number was 0.25. The LOLEX method was used for curvature and normal vector calculation. A comparison of the experimental and simulation results are shown in Figure 15.

The time intervals between frames for the experimental and simulation results do not match in this figure. The intervals between the second and third frames are the ones that match best, suggesting that the behaviour of the thin air film that forms between the droplet and the pool before coalescence is the major source of this discrepancy. The grid used in the simulation is unable to resolve the thin film. It is not clear that an increased grid resolution would amend this, as the continuum approximation may not be valid for the thin air film. The width of this film is not known from experiments.

As an order-of-magnitude estimate, we can use the results by Hodgson and Lee [41]. They report that the width of the thin film between a droplet and a pool before merging, for the water-toluene system they study, is around $L = 100$ nanometers. Since the mean free path in air at room temperature and atmospheric pressure is around $\lambda = 66$ nanometers [43], the Knudsen number is $Kn = \frac{\lambda}{L} \approx 0.7 \not\ll 1$, which would imply that the continuum description is no longer valid.

Nevertheless, the simulation is able to correctly predict the partial coalescence, and the simulation agrees well with experiments on the size of the daughter droplet produced. In the experiments, this daughter droplet subsequently bounces on the pool of water. The simulation is unable to predict this, again due to the thin air film formed, and shows the daughter droplet merging with the water pool instead.

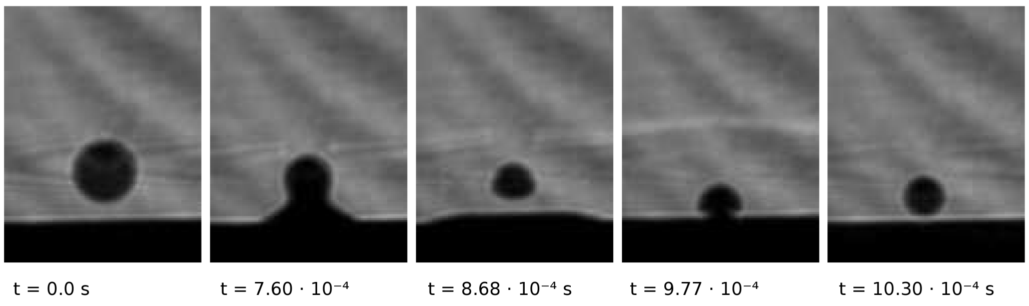

(a) Experimental result

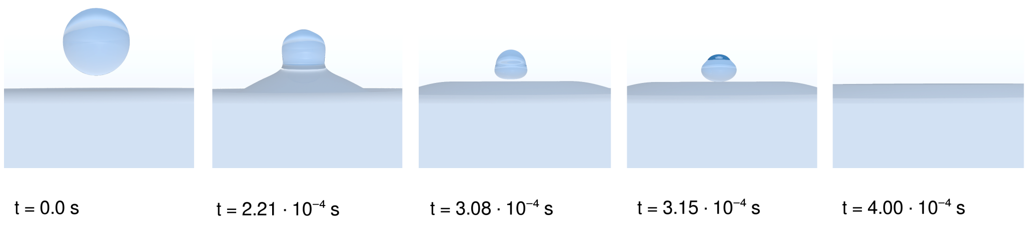

(b) Simulation result

Figure 15: Experimental results (top) and simulation results (bottom) for a 0.18 mm water droplet falling through air and impacting a deep pool of water at 0.29 m/s. Figure (a) is reprinted from [42], Copyright (2011), with permission from Elsevier.

A comparison between the LOLEX method and the standard method is shown in Figures 16 and 17. These figures show a section through the droplets just before collision and just when the neck is at its tallest, respectively. The pressure field is plotted as colored contours. The LOLEX method is plotted on the left side and the standard method is plotted on the right side. It is seen from these figures that the curvature errors produced by the standard method give rise to significant oscillations in the pressure; note in particular the interleaved red and blue patches where the pressure changes sign. As the reinitialization is performed more frequently, the oscillations persist, and are even found inside the pool below the droplet.

An important effect of this erroneous pressure is a loss of kinetic energy, which can be seen in Figure 17, where the neck is clearly shorter with the standard method. It is also seen that more frequent reinitialization leads to a higher loss of kinetic energy. As some authors have noted [44], the height of the neck and the dynamics of the capillary waves are important factors for the partial coalescence mechanism.

The LOLEX method is not significantly affected by the amount of reinitialization, and gives a more sensible pressure field in both cases. It should be noted that the pressure difference across the droplet interface in Figure 16 is about 2500 Pa, which is very large, caused by the very small droplet diameter.

This case also allows an illustration of the benefit of using the LOLEX method over the Salac and Lu method. In Figure 18 we compare the curvature field for these two just after droplet-film merging, where it is seen that curvature errors in the Salac and Lu method have led to the entrainment of a small bubble. Since the bubble is under-resolved on this grid, it subsequently disappears due to reinitialization. The LOLEX method does not entrain any bubbles.

Finally, we consider the performance impact of the LOLEX method on this case. The same simulations using the LOLEX and standard method were rerun using a 201×201 grid for timing purposes. The simulation using the standard method took 43525 s of CPU time, while the simulation using the LOLEX method took 46753 s. This means the LOLEX method is 7% slower than the standard method for this case, which is a fair trade-off for the benefits of both reduced pressure oscillations and lower sensitivity to reinitialization frequency.

6. Concluding remarks

In the present work we have proposed a new method for calculating the curvature and normal vectors of an interface represented by a level-set function, and which gives accurate results before, during and after topological changes in the interface. The method is compared to the standard method for geometric test cases, where the analytical curvature is known, and it is seen that in areas where the standard method gives errors of around 100 %, the proposed method gives errors of around 1–2 %. The method is easily extended to 3D, as is demonstrated, where the same reduction in error is seen. The method is then employed in simulations of two-phase flow where a droplet merges with a pool. Here it is seen that the standard method gives rise to unphysical pressure oscillations before merging, which affect the subsequent capillary waves, while the proposed method fares much better. The results of the simulations using the proposed method are compared to experimental results both for a liquid-in-liquid case, where the agreement is very

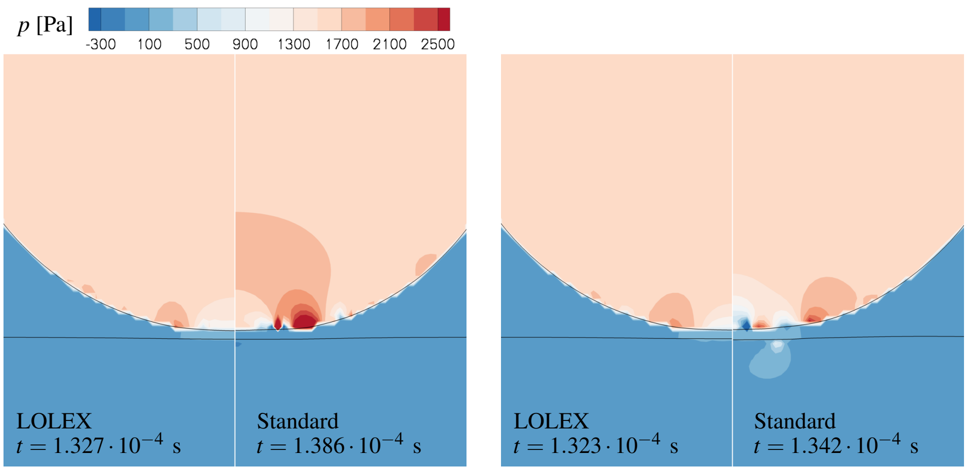

(a) Reinitialization every 7 time steps

(b) Reinitialization every time step

Figure 16: Water droplet falling onto a pool, just before the interfaces merge. Comparison between the LOLEX method and the standard method. The pressure field is shown as colored contours.

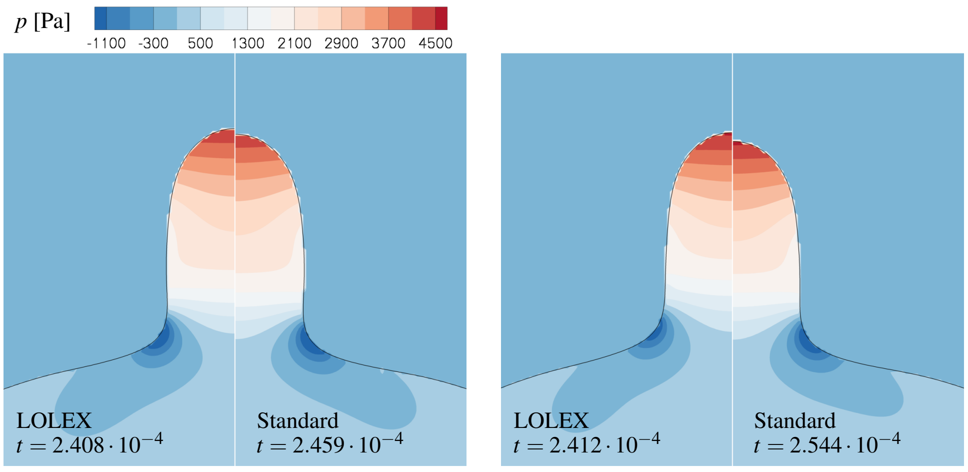

(a) Reinitialization every 7 time steps

(b) Reinitialization every time step

Figure 17: Water droplet falling onto a pool, when the neck reaches its highest position. Comparison between the LOLEX method and the standard method. The pressure field is shown as colored contours.

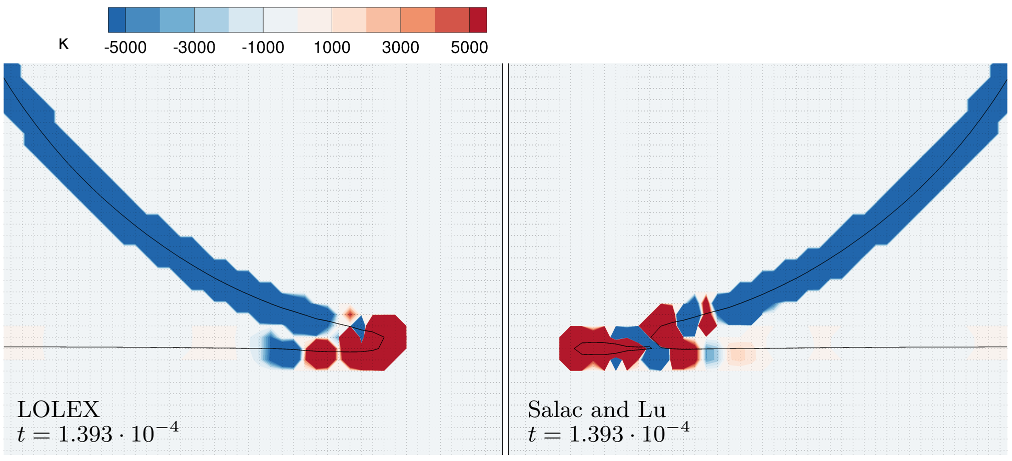

Figure 18: Water droplet falling onto a pool, zoom in on the interface just after merging. Comparison between the LOLEX method and the Salac and Lu method. It is seen that the latter entrains a small air bubble due to the oscillatory curvature field following the merging. The curvature field is shown as colored contours.

good, and for a more demanding liquid-in-gas case where the agreement is qualitative, reproducing the partial coalescence behaviour.

Acknowledgements

This work was financed through the Enabling Low-Emission LNG Systems project at SINTEF Energy Research, and the authors acknowledge the contributions of GDF SUEZ, Statoil and the Petromaks programme of the Research Council of Norway (193062/S60). We also thank one of the anonymous reviewers for detailed and extensive comments which helped improve the quality of this work.

References

[1] L. Rayleigh, in: Proc. R. Soc., 28, p. 406.
[2] A. M. Worthington, in: Proc. R. Soc., 25, pp. 261–272.
[3] S. T. Thoroddsen, K. Takehara, T. G. Etoh, S. Popinet, P. Ray, C. Josserand, S. Zaleski, M.-J. Thoraval, von Kármán vortex street within an impacting drop, Phys. Rev. Lett. 108 (2012) 264506.
[4] P. Macklin, J. Lowengrub, Evolving interfaces via gradients of geometry-dependent interior Poisson problems: application to tumor growth, Journal of Computational Physics 203 (2005) 191 – 220.
[5] V. Mallet, D. Keyes, F. Fendell, Modeling wildland fire propagation with level set methods, Computers and Mathematics with Applications 57 (2009) 1089 – 1101.
[6] V. Melicher, I. Cimrak, R. V. Keer, Level set method for optimal shape design of MRAM core. Micromagnetic approach, Physica B: Condensed Matter 403 (2008) 308 – 311.
[7] S. Osher, R. P. Fedkiw, Level set methods: An overview and some recent results, Journal of Computational Physics 169 (2001) 463 – 502.
[8] S. Osher, J. A. Sethian, Fronts propagating with curvature-dependent speed: Algorithms based on Hamilton-Jacobi formulations, Journal of Computational Physics 79 (1988) 12 – 49.
[9] P. Smereka, Semi-implicit level set methods for curvature and surface diffusion motion, Journal of Scientific Computing 19 (2003) 439–456.

[10] P. Macklin, J. Lowengrub, An improved geometry-aware curvature discretization for level set methods: Application to tumor growth, Journal of Computational Physics 215 (2006) 392 – 401.

[11] D. Salac, W. Lu, A local semi-implicit level-set method for interface motion, Journal of Scientific Computing 35 (2008) 330–349.

[12] K. Y. Lervåg, Calculation of interface curvature with the level-set method, in: Sixth National Conference on Computational Mechanics MekIT'11, Trondheim, Norway.

[13] K. Y. Lervåg, B. Müller, S. T. Munkejord, Calculation of the interface curvature and normal vector with the level-set method, Computers and Fluids 84 (2013) 218–230.

[14] Åsmund Ervik, The local level-set extraction method for robust calculation of geometric quantities in the level-set method, Master's thesis, Norwegian University of Science and Technology (NTNU), 2012.

[15] S. O. Unverdi, G. Tryggvason, A front-tracking method for viscous, incompressible, multi-fluid flows, Journal of Computational Physics 100 (1992) 25 – 37.

[16] D. Hartmann, M. Meinke, W. Schröder, The constrained reinitialization equation for level set methods, Journal of Computational Physics 229 (2010) 1514 – 1535.

[17] J. E. Pilliod, Jr., E. G. Puckett, Second-order accurate volume-of-fluid algorithms for tracking material interfaces, Journal of Computational Physics 199 (2004) 465 – 502.

[18] M. Sussman, K. Smith, M. Hussaini, M. Ohta, R. Zhi-Wei, A sharp interface method for incompressible two-phase flows, Journal of Computational Physics 221 (2007) 469 – 505.

[19] S. Shin, I. Yoon, D. Juric, The local front reconstruction method for direct simulation of two- and three-dimensional multiphase flows, Journal of Computational Physics 230 (2011) 6605–6646.

[20] D. Peng, B. Merriman, S. Osher, H. Zhao, M. Kang, A PDE-based fast local level set method, Journal of Computational Physics 155 (1999) 410 – 438.

[21] M. Kang, R. P. Fedkiw, X.-D. Liu, A boundary condition capturing method for multiphase incompressible flow, Journal of Scientific Computing 15 (2000) 323–360.

[22] E. B. Hansen, Numerical simulation of droplet dynamics in the presence of an electric field, Ph.D. thesis, Norwegian University of Science and Technology (NTNU), 2005.

[23] M. Sussman, P. Smereka, S. Osher, A level set approach for computing solutions to incompressible two-phase flow, Journal of Computational Physics 114 (1994) 146 – 159.

[24] R. P. Fedkiw, X. D. Liu, The Ghost Fluid Method for viscous flows, Presented at the "Solutions of PDE" Conference in honour of Prof. Phil Roe, 1998.

[25] A. Chorin, Numerical solution of the Navier–Stokes equations, Math. Comp 22 (1968) 745–762.

[26] S. Balay, J. Brown, K. Buschelman, W. D. Gropp, D. Kaushik, M. G. Knepley, L. C. McInnes, B. F. Smith, H. Zhang, PETSc Web page, 2012. http://www.mcs.anl.gov/petsc.

[27] J. Kraaijevanger, Contractivity of Runge–Kutta methods, BIT Numerical Mathematics 31 (1991) 482–528.

[28] D. I. Ketcheson, A. C. Robinson, On the practical importance of the SSP property for Runge–Kutta time integrators for some common Godunov-type schemes, International Journal for Numerical Methods in Fluids 48 (2005) 271–303.

[29] G.-S. Jiang, C.-W. Shu, I. L, Efficient implementation of weighted ENO schemes, J. Comput. Phys 126 (1996) 202–228.

[30] K. Y. Lervåg, Å. Ervik, Curvature calculations for the level-set method, in: ENUMATH 2011 Proceedings Volume, Leicester, England.

[31] C. Focke, D. Bothe, Direct numerical simulation of binary off-center collisions of shear thinning droplets at high Weber numbers, Physics of Fluids 24 (2012) 73105.

[32] P. Trontin, S. Vincent, J. Estivalezes, J. Caltagirone, A subgrid computation of the curvature by a particle/level-set method. application to a front-tracking/ghost-fluid method for incompressible flows, Journal of Computational Physics 231 (2012) 6990 – 7010.

[33] P. Verbeek, L. van Vliet, J. van de Weijer, Improved curvature and anisotropy estimation for curved line bundles, in: Jain, AK and Venkatesh, S and Lovell, BC (Ed.), Fourteenth International Conference on Pattern Recognition, Vols 1 and 2, International Conference on Pattern Recognition, pp. 528–533.

[34] D. Adalsteinsson, J. A. Sethian, A fast level set method for propagating interfaces, Journal of Computational Physics 118 (1995) 269 – 277.

[35] D. Adalsteinsson, J. A. Sethian, The fast construction of extension velocities in level set methods, Journal of Computational Physics 148 (1999) 2 – 22.

[36] Z. Mohamed-Kassim, E. K. Longmire, Drop impact on a liquid–liquid interface, Physics of Fluids 15 (2003) 3263–3273.

[37] P. Flynn, A. Jain, On reliable curvature estimation, in: Computer Vision and Pattern Recognition,

1989. Proceedings CVPR ’89., IEEE Computer Society Conference on, pp. 110 –116.

[38] C.-K. Tang, G. Medioni, Curvature-augmented tensor voting for shape inference from noisy 3D data, Pattern Analysis and Machine Intelligence, IEEE Transactions on 24 (2002) 858 –864.

[39] X. Chen, S. Mandre, J. J. Feng, Partial coalescence between a drop and a liquid-liquid interface, Physics of Fluids 18 (2006) 051705.

[40] Z. Mohamed-Kassim, E. K. Longmire, Drop coalescence through a liquid/liquid interface, Physics of Fluids 16 (2004) 2170–2181.

[41] T. Hodgson, J. Lee, The effect of surfactants on the coalescence of a drop at an interface i, Journal of Colloid and Interface Science 30 (1969) 94 – 108.

[42] H. Zhao, A. Brunsvold, S. T. Munkejord, Transition between coalescence and bouncing of droplets on a deep liquid pool, International Journal of Multiphase Flow 37 (2011) 1109–1119.

[43] S. G. Jennings, The mean free path in air, Journal of Aerosol Science 19 (1988) 159–166.

[44] F. Blanchette, T. P. Bigioni, Partial coalescence of drops at liquid interfaces, Nature Physics 2 (2006) 254–257.